Radiation Measurements 192 (2026) 107614

Contents lists available at ScienceDirect

Radiation Measurements

journal homepage: www.elsevier.com/locate/radmeas

# Optical response characterization of dyed-polymethyl methacrylate (PMMA) dosimeters under high-dose X-ray irradiation ☆

Y.Q. Aguiar [a,b,*], M. Avesani [a], A. Raj Mandal [a], X. Li [c], V. Hutanu [c], A. Morana [a], R. García Alía [b], S. Girard [a,d], M. Ferrari [a]

[a] Université Jean Monnet Saint-Etienne, CNRS, Laboratoire Hubert Curien UMR 5516, Saint-Etienne, F-42023, France
[b] European Organisation for Nuclear Research (CERN), Geneve, CH-1211, Switzerland
[c] Research Neutron Source Heinz Maier-Leibnitz (FRM II), TUM, Garching, 85748, Germany
[d] Institut Universitaire de France (IUF) Ministère de l'Enseignement Supérieur et de la Recherche, Paris, 75005, France

ARTICLE INFO

*Keywords:*
Dosimetry
Polymethyl methacrylate (PMMA)
Radiophotoluminescence (RPL)
Radiation-induced attenuation (RIA)
Transmittance

ABSTRACT

This study assesses the suitability of commercial dyed polymethyl methacrylate (PMMA) dosimeters for high-dose radiation applications extending into the hundreds of kilograys. Three PMMA dosimeter types (Gammachrome YR+, Amber 3042, and Red 4034) were investigated using both online and post-irradiation optical transmission measurements in the visible spectral range. The objective was to evaluate their dose sensitivity beyond nominal operational limits and to characterize their optical response through multi-wavelength transmittance and radiation-induced attenuation (RIA) analyses. Dosimeters were exposed to X-rays at dose rates of 0.9 and 1.2 Gy[$H_2O$]/s, covering doses from 0.1 Gy to 282 kGy. Monte Carlo simulations using the PHITS code were performed to model radiation transport and dose deposition in the different materials. The results demonstrate a clear, dose-dependent optical response of dyed PMMA, with wavelength-specific behavior indicative of color-center formation and evolution. Recovery measurements show that the RIA signal is highly stable over several hours at nominal wavelengths, with only minor relaxation observed in the near-infrared region, supporting the applicability of these dosimeters for both real-time and passive measurements. Comparisons with Radiophotoluminescent (RPL) FD-7 dosimeters reveal consistent trends, suggesting the potential for establishing a conversion between RPL and PMMA dose responses. Overall, the findings support the extension of dyed-PMMA dosimetry beyond current commercial limits and contribute to the development of robust dosimetry techniques for extreme radiation environments.

## 1. Introduction

The use of ionizing radiation is increasingly integral to a wide range of industrial and medical applications, including sterilization of medical devices, food preservation, polymer modification, and radiation processing. Furthermore, radiation exposure levels in extreme environments such as particle accelerators, fission reactors, and nuclear waste repositories have steadily increased over the past decade, a trend expected to continue in the foreseeable future (Girard et al., 2018; Macha et al., 2025). These developments have driven the demand for extending the operational range and real-time capabilities of existing dosimetry systems through enhanced detection methods and broadband readout techniques (Camanzi and Holmes-Siedle, 2008; Pramberger et al., 2022).

Dosimetry systems quantify absorbed dose through the detection of radiation-induced physical or chemical changes in specific materials. Commonly used detection mechanisms include optical density variations in polymethyl methacrylate (PMMA) and radiochromic films, as well as radiophotoluminescence and transmittance measurements in phosphate-based glass dosimeters (Pramberger et al., 2022; Khan et al., 1988; Devic, 2011; Attix, 1986; Rieker et al., 2025). Among these, PMMA dosimeters are widely adopted in industrial gamma processing environments due to their robustness and simple optical readout procedures (Barret, 1982; Miller et al., 1975). These dosimeters are available in both undyed and dyed formulations. In undyed PMMA dosimeters, radiation exposure leads to the formation of degradation products that absorb in the ultraviolet (UV) region, typically between 300 nm and 320 nm. In constrat, dyed PMMA incorporates radiation-sensitive chromophores into the polymer matrix. Upon irradiation, free radicals interact with these dye molecules, forming stable color centers.

☆ This article is part of a Special issue entitled: 'SSD21' published in Radiation Measurements.

* Corresponding author at: European Organisation for Nuclear Research (CERN), Geneve, CH-1211, Switzerland.
*E-mail address:* ygor.aguiar@cern.ch (Y.Q. Aguiar).

https://doi.org/10.1016/j.radmeas.2026.107614
Received 31 October 2025; Received in revised form 16 December 2025; Accepted 7 January 2026
Available online 9 January 2026

These centers exhibit characteristic absorption in the visible spectrum, enabling dose quantification via spectrophotometric measurements.

Radiophotoluminescent dosimeters (RPLDs), such as those based on FD-7 phosphate glass, offer an alternative approach to dose measurement. Compact, passive, and capable of high-resolution dose measurements, RPLDs are widely adopted in clinical and personal dosimetry due to their low energy dependence, excellent long-term stability, and non-destructive readout capabilities. Beyond these applications, similarly to PMMA dosimeters, RPLDs have demonstrated strong performance in high-dose radiation environments as well, where their ability to form stable radiation-induced color centers becomes advantageous (Becker, 1973; Huang and Hsu, 2011; Yamamoto, 2011; Okada et al., 2022; Pramberger et al., 2022). RPLDs have demonstrated satisfactory response up to megagray (MGy) regimes and are currently employed in environments such as CERN to assess the radiation hardness of materials and electronics (Pramberger et al., 2022; Biłko et al., 2023; Aguiar et al., 2025; Ferrari et al., 2023).

In this study, we investigate the performance of dyed PMMA dosimeters across and beyond their standard calibration range and benchmark their response against FD-7 RPL dosimeters. Post-irradiation optical absorbance in the visible region was measured after irradiation with X-rays. Monte Carlo simulations using PHITS version 3.34 (Sato et al., 2024) were employed to investigate radiation transport and dose deposition within the dosimetric materials. In addition, spectral dependencies arising from radiation-induced attenuation (RIA) and photoluminescence are also evaluated. The findings aim to enhance high-dose dosimetry capabilities, particularly for industrial applications and high-energy accelerator environments.

## 2. Dyed-PMMA and RPL dosimeters

### 2.1. PMMA dosimetry

Polymethylmethacrylate (PMMA) dosimeters are widely used for high-dose gamma and X-ray measurements in industrial radiation processing due to their reliability, ease of use, and straightforward optical readout mechanisms. The dosimetric response of PMMA is governed by radiation-induced chemical transformations in the polymer matrix.

When exposed to ionizing radiation, PMMA polymer undergoes main-chain scission, which results in the formation of free radicals and various degradation products. In dyed-PMMA variants, these radiation-induced radicals interact with embedded dye molecules, giving rise to chromophores that absorb light in the visible spectrum in a dose-dependent manner. In Fig. 1, the commercial Harwell PMMA dosimeters are shown. For instance, the Red 4043 dye exhibits a prominent absorption band in the 600–650 nm range (Barret, 1982; Miller et al., 1975). In contrast, undyed PMMA shows absorbance primarily in the ultraviolet (UV) region (300–320 nm), and this phenomenon is attributed to the accumulation of polymer degradation products with dose rather than dye-radical interactions (Barret, 1982; Boag et al., 1958; Chapiro, 1956).

To ensure reproducibility and optical stability, dyed-PMMA dosimeters are manufactured under tightly controlled environmental conditions, including specific humidity and temperature constraints, and are often sealed in protective foils. Their response is sensitive to extrinsic factors such as ambient conditions and post-irradiation fading, as well as intrinsic factors like batch-to-batch variations (Miller et al., 1975). As a result, the use of these dosimeters requires rigorous and well-characterized calibration protocols (Barret, 1982; Glover et al., 1993; Fitriana and Putri, 2020). The incorporation of dye molecules mitigates post-irradiation bleaching and enhances color stability, making dyed dosimeters suitable for industrial dosimetry applications reaching into the tens of kilogray (kGy) dose range (Barret, 1982).

Optical absorbance measurements using a spectrophotometer at specific wavelengths remain the primary method for quantifying radiation-induced changes in PMMA dosimeters. In dyed-PMMA systems, the

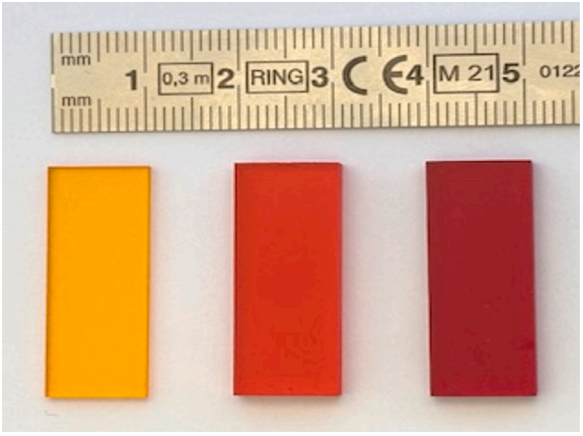


**Fig. 1.** Harwell perplex PMMA sample types (from left to right): Gammachrome YR+, Amber 3042 and Red 4034.

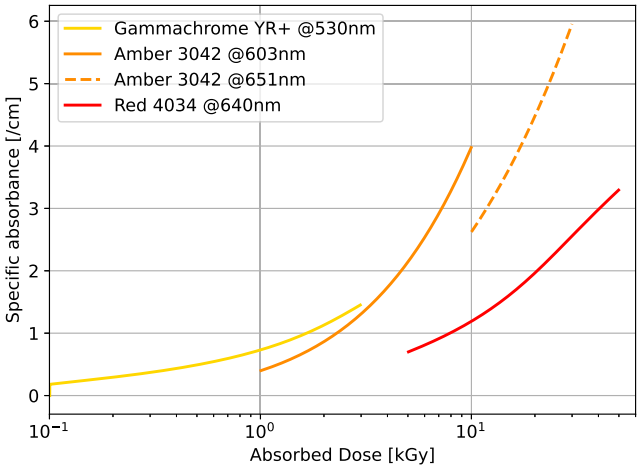


**Fig. 2.** Calibration curves provided by Harwell for the three PMMA sample types: Gammachrome YR+, Amber 3042 and Red 4034.

increase in absorbance at selected wavelengths within the visible spectrum provides a direct and reliable correlation to the absorbed dose. Calibration curves, such as those developed for Harwell PMMA dosimeters (see Fig. 2), establish this correlation and enable dose quantification. To ensure accurate comparisons across samples of varying thicknesses, absorbance is typically normalized to the optical path length. The resulting specific absorbance, defined as $k = A/t$ where $A$ is absorbance or optical density, and $t$ is optical path length or dosimeter thickness, is reported in units of $cm^{-1}$.

The baseline optical density before irradiation must be recorded to account for intrinsic absorption and potential batch-to-batch variability. Environmental conditions, such as temperature and humidity, and intrinsic parameters such as dosimeter thickness, must be taken into account during analysis to improve accuracy (Barret, 1982).

PMMA dosimeters are typically calibrated using irradiation conditions as close as possible to the intended application. This involves exposing dosimeters to known doses, typically from standardized $^{60}Co$ gamma or X-ray sources, and establishing calibration curves based on their optical response. Due to inherent sensitivity to environmental factors and manufacturing variability, recalibration is advised following any significant change in storage, handling, or irradiation conditions. When exploring the use of PMMA dosimeters for high-dose applications, beyond the producer's declared limits, it is essential to assess both the dose dependence of optical absorbance and the dynamic range of the dosimeter response, as saturation or non-linear behavior can occur

beyond specific thresholds (Barret, 1982). Typically, the wavelengths selected for dosimetry correspond to regions of the spectrum where the optical response exhibits the highest sensitivity, i.e. the largest variation with dose in the intended measurement range. While this maximizes signal-to-noise and measurement precision, it also implies that these wavelengths can reach saturation at high doses more quickly than other wavelengths. Therefore, evaluating the full spectral absorbance evolution across the visible range is valuable, as it may reveal alternative wavelengths with usable sensitivity, providing a possible route to extend the dosimeter's dynamic range and maintain accurate dose assessment even in regimes where the primary wavelength saturates.

### 2.2. RPL dosimetry

Radiophotoluminescence (RPL) dosimeters are passive detectors that have gained increasing popularity due to their high sensitivity, stability, and versatility across a wide range of radiation environments, including mixed fields and high-dose scenarios (Pramberger et al., 2022; Becker, 1973; Huang and Hsu, 2011; Yamamoto, 2011; Okada et al., 2022). RPL dosimeters, typically made of Ag-doped phosphate glass (e.g., FD-7), operate on the principle of radiophotoluminescence, where ionizing radiation induces the formation of RPL centers and clusters (such as $Ag^0$ or $Ag^{2+}$) in the glass matrix. These centers can be excited with ultraviolet light causing luminescence at characteristic wavelengths. Within certain dose ranges, typically up to hundreds of Gy, the intensity of the emitted light is proportional to the absorbed dose, allowing quantitative RPL-based dose measurements (Yamamoto, 2011).

The readout of RPL dosimeters is performed using non-destructive readout techniques. Typically, a UV or blue light source excites the Ag centers, and the resulting photoluminescence is measured with a photomultiplier or spectrometer. This non-destructive approach allows repeated measurements to be performed without affecting the accumulated dose measurement. This is particularly advantageous for long-term follow-up after irradiation. Radiation-induced absorption (RIA) in the visible spectrum can also be measured to assess dose-dependent changes in optical properties, typically becoming relevant at higher doses, in the kGy range.

RPL dosimeters are calibrated using reference radiation sources, commonly $^{60}$Co gamma rays, to establish the relationship between luminescence intensity and absorbed dose. Calibration accounts for factors such as dose rate, temperature, and radiation energy spectrum. Conversion factors can be applied to estimate dose in different materials, which is particularly important when dosimeters are used in neutron-dominated or mixed radiation fields (Ferrari et al., 2024; Avesani et al., 2025). RPLDs show excellent stability against fading and environmental influences, although some non-linearities or dose-rate dependencies may still arise and warrant characterization at extremely high doses or in fast irradiation scenarios characterized by very high dose rates (Pramberger et al., 2022; Aguiar et al., 2025).

Compared to PMMA dosimeters, RPL dosimeters are highly effective at low doses and are explicitly designed for measurements up to roughly 100 Gy. Extending their use to higher doses requires combining traditional RPL readout with transmission measurements, but in this regime the fundamental dosimetric mechanism shifts to a complex relationship between different optical center concentrations. This necessitates additional excitation sources, modified readout systems, and re-characterization of the dose response (Pramberger et al., 2022). By contrast, PMMA dosimeters are inherently suitable for high-dose applications, with nominal ranges extending to tens of kGy. Building on the successful optical readout strategies developed for RPL dosimeters, the present study explores applying the same approach to dyed-PMMA systems, aiming to extend their applicability while retaining the same dosimetric principle, formation of radiation-induced color centers, without major modifications to the measurement system.

## 3. Methodology

### 3.1. Dosimeter samples

In this study, three commercially available dyed polymethyl methacrylate (PMMA) Harwell dosimeters were selected for high-dose radiation characterization (shown in Fig. 1). These dosimeters, namely Gammachrome YR+, Amber 3042, and Red 4034, are designed for gamma and X-ray processing environments and are each calibrated for specific dose ranges and wavelengths of optical transmission, as shown in Table 1. The measurement wavelengths correspond to the peak absorbance bands of each dye type, as provided by the manufacturer and confirmed by spectrophotometric analysis. For Amber 3042, two wavelengths are used depending on the dose range, 603 nm from 1 to 10 kGy and 651 nm from 10 kGy to 30 kGy.

Each of these dosimeter types is manufactured under strict quality control protocols. Prior to distribution, they are calibrated using a standardized cobalt-60 gamma irradiator and verified through spectrophotometric absorbance measurements. The coefficient of variation in specific absorbance values is maintained below 2.5%, ensuring batch-to-batch uniformity (Harwell Dosimeters Ltd., 2024). All calibrations and irradiator operations are traceable to national measurement standards in the United Kingdom. The absorbed dose is estimated using the calibration curves provided by the producer and shown in Fig. 2. The three dosimeter types used in this work are shown in Fig. 1.

To provide a comparative benchmark, radiophotoluminescence (RPL) FD-7 dosimeters were also employed. These dosimeters are part of the GD-301 series manufactured by Chiyoda Technol Corporation (Japan) and consist of silver-doped phosphate glass rods. The cylindrical glass rods have a diameter of 1.5 mm and a length of 8.5 mm. Their nominal composition includes phosphorus (31.55 wt %), oxygen (51.16 wt %), aluminum (6.12 wt %), sodium (11 wt %), and silver (0.17 wt %), as previously reported in the literature (McKeever, 2022). In standard commercial configuration, the glass rod is embedded in a plastic housing. For the experiments described here, the glass rod was carefully removed from its container to characterize its optical response alone. In the context of this study, the term RPL dosimeter refers exclusively to the bare FD-7 glass rod. The performance of these dosimeters under high-dose conditions has been extensively documented in earlier work (Pramberger et al., 2022; Ferrari et al., 2024; Raj Mandal et al., 2025; Aguiar et al., 2025).

### 3.2. Irradiation setup

As illustrated in Fig. 3, a custom-built experimental setup was developed for real-time (online) light transmission measurements (Hasan et al., 2024; Raj Mandal et al., 2025). This configuration allows for transmission of multi-wavelength broadband light through the dosimeter sample during irradiation. The setup consists of a deuterium-halogen white light source (DH-2000, Ocean Optics) and a high-resolution spectrometer (QE-Pro 38011, Ocean Optics), optimized for the detection of wavelengths in the range of 240 nm to 1000 nm. Light from the source is transmitted via a high-hydroxyl content, pure silica-core transport fiber, optimized for transmission in the ultraviolet–visible range. A metallic-coated mirror serves as a collimator, directing the beam through the dosimeter sample positioned on a custom holder. On the opposite side, a second collimator collects the transmitted light and channels it to the spectrometer via a second optical fiber of identical type.

In the online measurement configuration, the sample, sample holder, and optical collimators are placed inside the X-ray chamber, while the white light source and spectrometer are located out of the irradiator chamber, to remain shielded. PMMA samples are placed vertically with the light beam focused perpendicularly to the largest surface of the dosimeter, as shown in Fig. 3. The system records transmitted optical intensity at a selected acquisition rate, enabling the measurement of

**Table 1**
Characteristics of dyed PMMA dosimeters with measurement wavelength provided by Harwell and the characteristics of the FD7 RPL dosimeter used in this study.

| | Gammachrome YR+ | Amber 3042 | Red 4034 | RPL FD7 |
|---|---|---|---|---|
| Nominal dose range | 0.1–3 kGy | 3–30 kGy | 5–50 kGy | up to MGy |
| Measurement wavelength | 530 nm | 603/651 nm | 640 nm | 365 and 440 nm |
| Thickness | 1.7 mm | 3 mm | 3 mm | 1.5 mm |
| Size | 30 x 11 mm | 30 x 11 mm | 30 x 11 mm | 8.5 x 1.5 mm |
| Color change | Yellow → Red | Amber → Brown | Red → Dark Red | Transparent → Yellow |

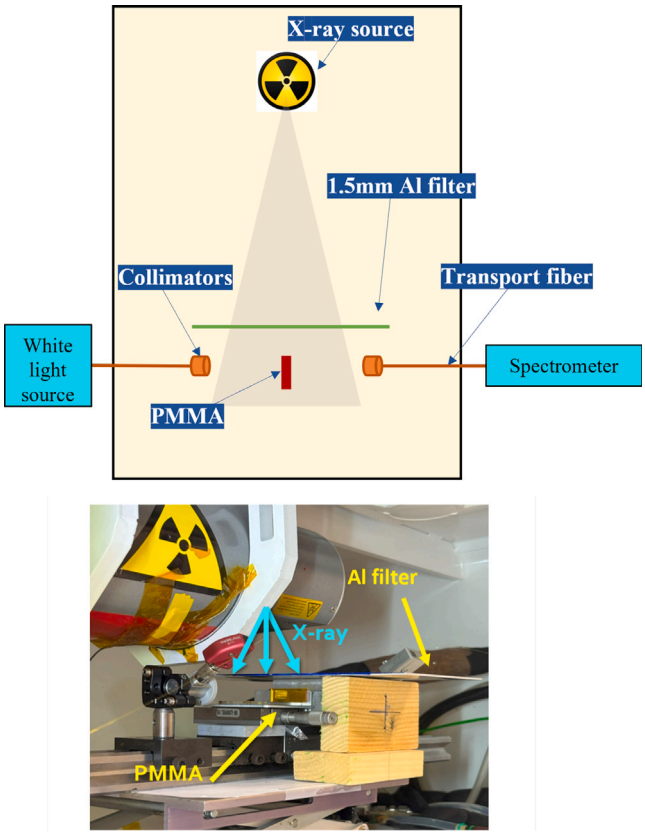


**Fig. 3.** Schematic diagram of the experimental setup for online RIA measurements. PMMA samples are positioned vertically with the light beam perpendicular to the largest surface of the dosimeter.

radiation-induced absorption (RIA) as a function of dose and wavelength. RIA is calculated at any point in time using the following relation:

$$RIA\,(t,\lambda) = -\left(\frac{10}{L}\right)\cdot \log_{10}\left(\frac{\mathrm{I}(t,\lambda)-\mathrm{I_N}(\lambda)}{\mathrm{I_{ref}}(0,\lambda)-\mathrm{I_N}(\lambda)}\right) \quad (1)$$

Where $\mathrm{I_{ref}}(0,\lambda)$ represents the pre-irradiation transmitted signal at wavelength $\lambda$, and $\mathrm{I}(t,\lambda)$ signal at time $t$ during or after irradiation. $\mathrm{I_N}(\lambda)$ is the background signal due to thermal noise at the same wavelength. The sample length is denoted as $L$. All intensities are expressed in photon counts, integrated over a fixed acquisition time. RIA depends on various parameters including the absorbed dose, dose rate, temperature, wavelength, light intensity, and material composition, as previously reported in the literature (Girard et al., 2013, 2019).

When the transmitted signal is measured during irradiation, the resulting attenuation is referred to as online RIA. This measurement provides insight into the growth and evolution of absorption bands associated with radiation-induced defect centers. Such observations are not always accessible through conventional post-irradiation methods, which primarily capture long-lived defect states. Therefore, the online measurement technique is essential for understanding the complete optical response of dosimetric materials.

### 3.3. Irradiation conditions

The radiation source used in this study was operated on the PETRA (Girard et al., 2025) experimental platform at Laboratoire Hubert Curien in France. The MOPERIX X-ray irradiator, equipped with a tungsten target, was set to operate at 160 kV (Meyer et al., 2023). Absorbed dose values in this irradiation campaign range from 0.1 kGy to 282 kGy, measured in water-equivalent material. Two dose rates were selected for the experiments: 0.9 and 1.2 Gy[$H_2O$]/s at 20 ± 4 °C, and for a total duration ranging from 3 min to a maximum of 64 h of continuous irradiation. Dose rates are modulated by adjusting the tube current.

Photons with lower energy in this spectrum are highly attenuated by the sample thickness, depositing most of their energy on the sample top layers and leading to a highly inhomogeneous dose distribution. As evidenced by Monte Carlo calculations using PHITS, the adoption of a 1.5 mm thick Al shielding, as shown in Fig. 3, was proven to effectively improve spectral hardness and improve dose homogeneity within the PMMA and RPL volume (Ferrari et al., 2024).

Reference dose-to-water at the sample position was measured using a PTW 23344 ionization chamber. In Avesani et al. (2025), a conversion factor $C_{sim}$ is reported which allows the readout of the ionization chamber to be converted in dose to RPL material $D_{RPL}$ in these irradiation conditions. $C_{sim}$ corresponds to 3.2 ± 0.2 (Avesani et al., 2025). In this work, RPLD dose values refer to dose to RPL material, and they are obtained with the following formula:

$$D_{RPL} = \dot{D_W} \cdot t_{irr} \cdot C_{sim} \quad (2)$$

where $\dot{D_W}$ is the dose rate in water measured with the ionization chamber at the irradiation position and $t_{irr}$ is the total irradiation time.

RPL dosimeters were positioned on both sides of the PMMA sample. PMMA samples were removed from their sealed packages and irradiated horizontally, except for online measurements, where they were placed vertically. For thicker amber and red PMMA types, samples were irradiated horizontally but flipped midway to ensure more uniform dose deposition on the dosimeter volume. Subsequent simulation results confirm improved depth-dose uniformity in these cases.

### 3.4. Monte Carlo simulations

Monte Carlo simulations were performed using the PHITS code to evaluate the energy deposition of X-rays in PMMA and to compute a conversion factor to assess the ratio between dose-to-water and dose-to-PMMA values in the selected irradiation conditions. Additionally, the simulations assessed the spatial uniformity of energy deposition within PMMA samples under the irradiation conditions detailed in Section 3.3. A schematic view of the simulated geometry is illustrated in Fig. 4. The X-ray source is modeled as a point emitting X-rays isotropically and located in the center of a vacuum chamber, with the PMMA sample positioned approximately 6 cm downstream of the source. The source energy spectrum was computed using SpekPy 2.0 (Poludniowski et al., 2021a) for 160 kV voltage with a 4 mm beryllum filter and a 1.5 mm aluminum filter useful to harden the spectrum. Comparing the spectrum

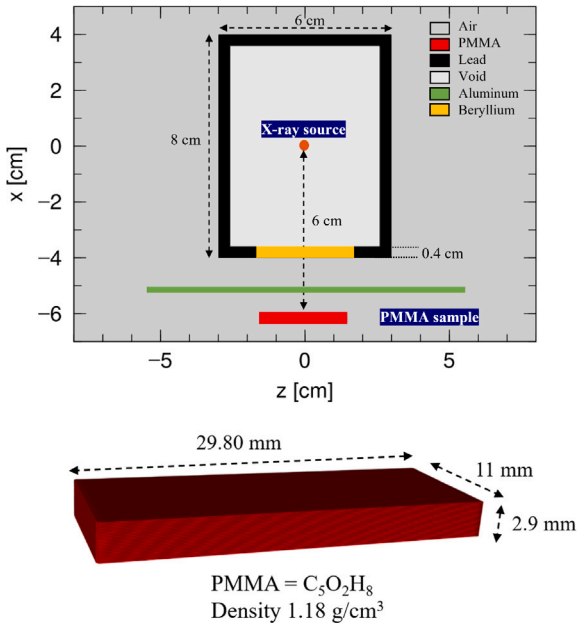


**Fig. 4.** PHITS simulation setup considering the horizontal placement of PMMA samples (offline measurements).

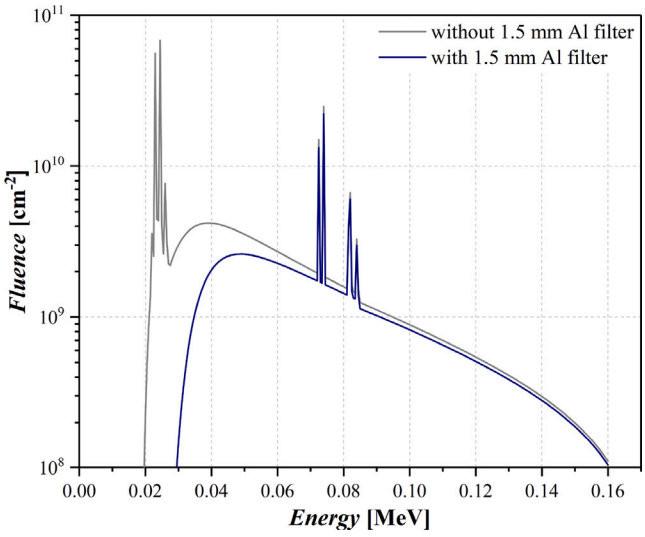


**Fig. 5.** Comparison of X-ray spectra obtained with a 4 mm Be filter, with (blue) and without (gray) an additional 1.5 mm Al filter, using the X-ray tube operated at 160 kV (Poludniowski et al., 2021b).

with (blue line) and without (gray line) a 1.5 mm-thick aluminum filter, shown in Fig. 5, in the filtered spectrum a notable suppression of low-energy photons is observed, improving penetration and minimizing near-surface dose peaks. The PMMA was simulated with a composition of $C_5H_8O_2$ and a density of 1.18 g/cm$^3$.

To analyze depth-dose uniformity, the PMMA volume was segmented into 0.1 mm thick slabs along the $x$ axis allowing for detailed profiling of fluence and energy deposition as a function of sample depth. For the first 15 slabs, corresponding to the 1.5 mm thickness of the Gammachrome YR+ dosimeter, the photon fluence decreased by approximately 6%. In contrast, the final slab, corresponding to the full 3 mm thickness of Amber and Red dosimeters, shows a fluence reduction of around 15%. To compensate for this gradient and improve dose uniformity of the 67% in thicker samples, the Amber 3042 and Red 4034 dosimeters were irradiated from both sides (flipped halfway through the exposure).

## 4. Results and discussion

Based on the deposited dose results, a conversion factor was derived to relate dose-to-water, obtained using in the simulation the same geometry as the one described for the PMMA but with the dosimeter made of water and dose-to-PMMA:

$$C_{Sim} = \frac{D_{PMMA}}{D_{Water}} \approx 0.73 \quad (3)$$

This factor was consistently applied to all PMMA dose evaluations in the present study, enabling a direct comparison of dose deposited in PMMA and water-equivalent dosimetry systems and ensuring a quantitative comparability with dose-to-water reference measurements. As discussed earlier, the factor accounts for both spectral differences and energy-dependent mass absorption characteristics of PMMA relative to water under X-ray irradiation. For all the performed simulations the computational errors of the scored results were below 5%, it can be assumed that the conversion factor is 0.73 ± 0.04.

### 4.1. Absorbance and transmission measurements

In this section, the results from the post-irradiation absorbance measurements using the Cary 6000i UV–Vis-NIR spectrophotomer (Agilent Technologies) are shown and discussed. Fig. 6 presents absorbance data at the wavelengths used for dosimetry for each of the PMMA dosimeters (as reported in Table 1). For each dyed-PMMA sample, absorbance was measured at two distinct locations on the sample surface (designated as point A and point B) to assess reproducibility, particularly in the case of passively irradiated samples. Since these samples were uniformly irradiated under well-controlled conditions, all surface points were assumed to be equivalent. Additionally, a second measurement was performed approximately one week after the first to evaluate the temporal stability of the readout after irradiation. Across the entire dataset, a high degree of consistency was observed, with variation remaining within 8%, even for samples exposed beyond their nominal calibration range. As expected, absorbance increased monotonically with absorbed dose for all PMMA types irradiated within their respective calibration windows. This trend is also observed in most of the PMMA irradiated out of the range. Notable exceptions were observed for the PMMAs irradiated actively (Amber 3042 at 50 kGy and Red 4034 at 280 kGy). These anomalies are attributed to less homogeneous dose deposition resulting from their vertical orientation during online irradiation measurement (as illustrated in Fig. 3). This effect is clearly observed in the transmission spectra of Amber 3042 irradiated vertically at 50 kGy, where measurements taken at different points on the sample surface (Fig. 7) show significant variation. The observed inhomogeneity contributed to larger discrepancies between measurement points (A and B) compared to the passively irradiated samples.

PMMA samples were irradiated either sealed inside the package or unsealed, in order to investigate the impact of the package during the irradiation since its role is to protect the dosimeter from humidity and other environmental condition, as previously mentioned. For instance, the Gammachrome YR+, Amber 3042 and Red 4034 samples irradiated at 2 kGy, 3.48 kGy and 20 kGy respectively were sealed. As shown in Fig. 6, the absorbance values of these sealed samples do not exhibit a different trend compared to those irradiated without their package, indicating negligible influence from packaging under the tested conditions.

Fig. 8 presents the spectral transmission behavior of each PMMA dosimeters irradiated at selected doses within and beyond their nominal calibration range. The transmission spectra show a clear dose-dependent decrease in optical transmission, attributed to the formation of radiation-induced color centers within the PMMA matrix. Compared

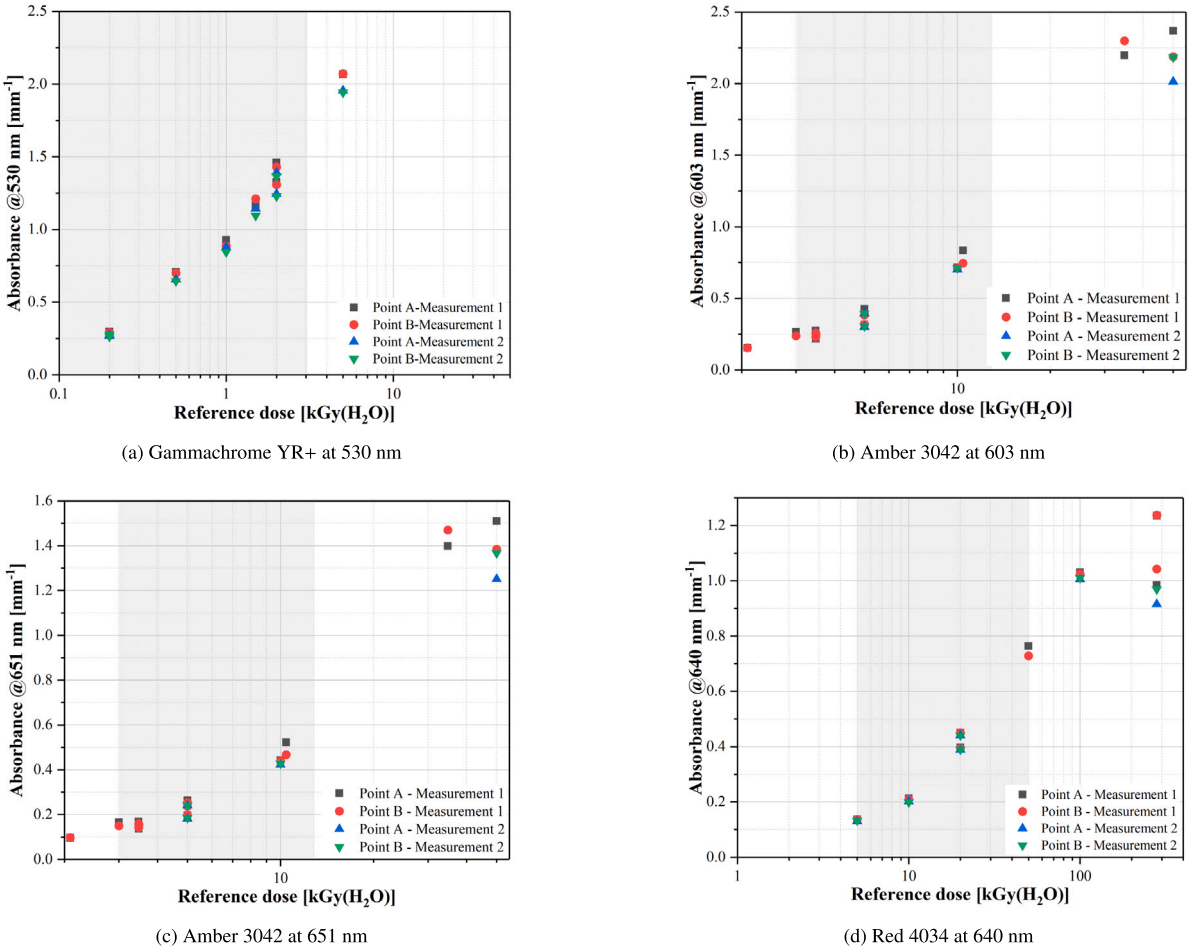


(a) Gammachrome YR+ at 530 nm

(b) Amber 3042 at 603 nm

(c) Amber 3042 at 651 nm

(d) Red 4034 at 640 nm

**Fig. 6.** Post-irradiation absorbance measured at characteristic dosimetry wavelengths for (a) Gammachrome YR+ @603 nm, (b) Amber 3042 @603 nm, (c) Amber 3042 @651 nm, and (d) Red 4034 @640 nm. Absorbance trends confirm dose-dependent optical response at target wavelengths.

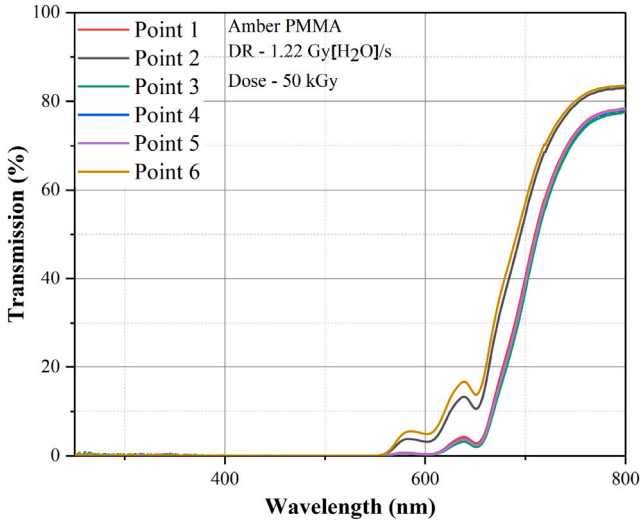


**Fig. 7.** Transmission spectra for several points within the Amber 3042 sample irradiated vertically at 50 kGy (online measurement configuration).

to the pristine state, the irradiated samples exhibit progressive darkening, particularly evident in the visible region between 500 and 800 nm. For example, as the dose increases from 2 to 50 kGy in Gammachrome YR+ samples, the transmission curve shifts toward longer wavelengths, with significant attenuation observed near the 530–580 nm range. This behavior is consistent with the accumulation of absorption bands linked to polymer degradation and dye radical interactions. In accordance with this, the values of the absorbance at 20 kGy, 50 kGy and higher doses are not reported in Fig. 6, as the measured absorbance is so low that it cannot be distinguish from the background noise, and are therefore considered unreliable. Similar responses are observed for Amber 3042 samples with significant attenuation near the 550–650 nm range and Red 4034 with significant attenuation near the 600–650 nm range.

### 4.2. Online RIA measurements

Fig. 9 displays RIA as a function of dose and time for selected wavelengths, measured online at a dose rate of 1.22 Gy[$H_2O$]/s. The RIA growth in Gammachrome YR+ sample (Fig. 9(a)) exhibits a strong spectral dependence, with shorter wavelengths (e.g., 530 and 570 nm) showing a steeper increase compared to longer wavelengths. At 580 nm, a substantial RIA signal is sustained up to 50 kGy, indicating the material's sensitivity and dynamic response across the visible range. For wavelengths above 600 nm, the RIA increase is less pronounced but still monotonic and measurable. While the RIA evolution at 530 nm confirms its usability for dosimetry up to few kGy, after which the absorption is too high to be measured with the used setup, the RIA evolution at longer wavelengths suggests that they can be possibly considered for Gammachrome PMMA extended usability up to tens of kGy. Similarly, the Amber 3042 sample exhibits steeper growth in RIA at 600 and 650 nm compared to longer wavelengths (see Fig. 9(b)). The

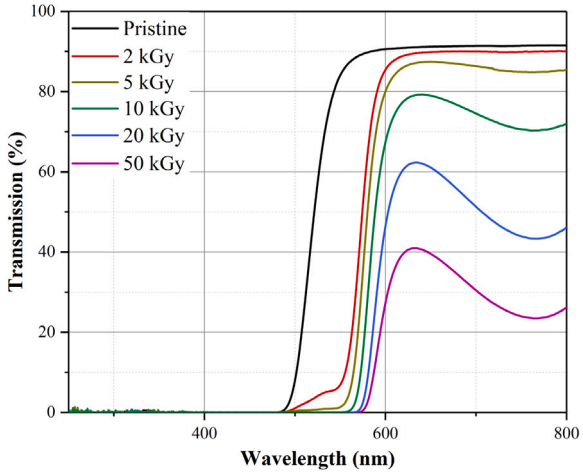


(a) Gammachrome YR+ at 2 kGy, 5 kGy, 10 kGy, 20 kGy and 50 kGy

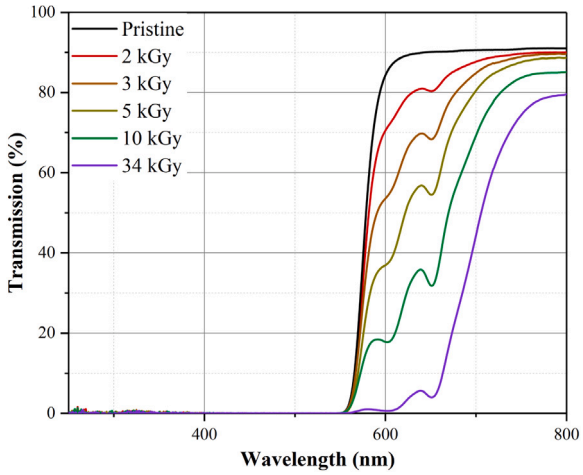


(b) Amber 3042 at 2 kGy, 3 kGy, 5 kGy, 10 kGy and 34 kGy

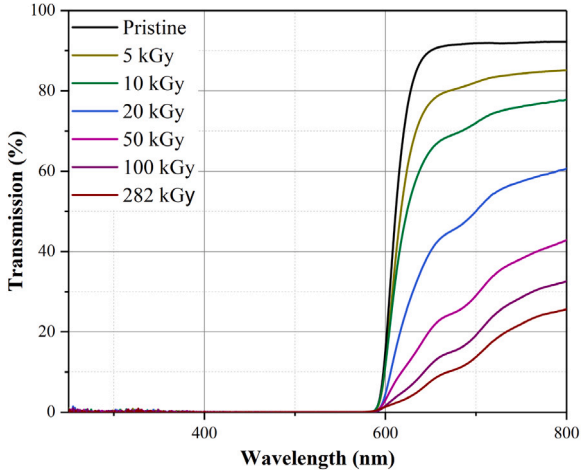


(c) Red 4034 at 5 kGy, 10 kGy, 20 kGy, 50 kGy, 100 kGy and 282 kGy

**Fig. 8.** Transmission spectra of (a) Gammachrome YR+, (b) Amber 3042, and (c) Red 4034 PMMA dosimeters after increasing doses. Increasing radiation dose results in visible darkening and spectral red-shifting.

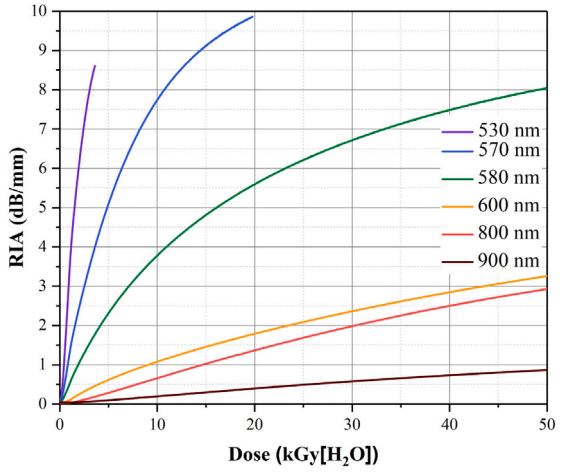


(a) Gammachrome YR+ up to 50 kGy

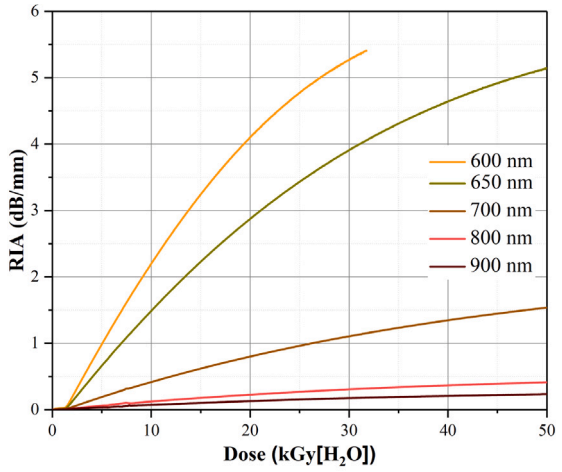


(b) Amber 3042 up to 50 kGy

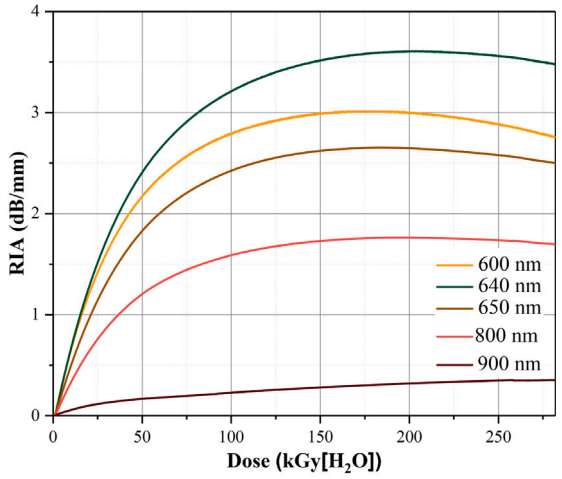


(c) Red 4034 up to 282 kGy

**Fig. 9.** Online RIA growth in (a) Gammachrome YR+, (b) Amber 3042, and (c) Red 4034 PMMA dosimeters at selected wavelengths during X-ray irradiation at a dose rate of 1.22 Gy[$H_2O$]/s. Higher RIA response is observed at shorter wavelengths.

RIA growth at longer wavelengths (e.g., 700 nm) remains monotonic, though less pronounced, indicating potential usability beyond the commercial calibration dose range. A similar trend is also observed for the Red 4034 sample. However, in this case, the RIA increases monotonically up to 50 kGy across all selected wavelengths as shown in Fig. 9(c), after which the growth slows down, reaches a saturation region, and eventually shows a slight decline beyond 200 kGy.

These results confirm the interest for further exploring PMMA dosimeter suitability for online dosimetry applications, offering reliable signal development with minimal post-irradiation fading across a wide dose interval.

### 4.3. Recovery kinetics

To assess the post-irradiation stability of the RIA signal, recovery kinetics were monitored for up to 3 h following exposure. Measurements were conducted in the irradiation chamber using the online setup, under ambient temperature and atmosphere laboratory conditions for all three dyed-PMMA types and results as shown in Fig. 10.

For the Gammachrome YR+ dosimeter irradiated to 50 kGy, minimal recovery was observed across the visible and near-infrared spectrum. At the wavelengths of 580 nm and 600 nm, the RIA signal decayed by less than 3%, indicating excellent temporal stability in this conditions, e.g. up to 3 h after irradiation. At longer wavelengths, minor relaxation was detected, approximately 0.3% at 700 nm, suggesting a more limited involvement of metastable defects at room temperature at this spectral position. A slight increase in the recovery at 800 nm is possibly due to instability of signal at longer wavelength, though the variation is lower than 0.4%. The Amber 3042 dosimeter, also irradiated to 50 kGy, exhibited exceptional stability at both wavelengths used for dosimetry. Specifically, the RIA signal at 620 nm and 650 nm decreased by less than 0.2% only, demonstrating negligible short-term fading. However, more pronounced recovery was observed at longer wavelengths, with less than 5% RIA reduction at 700 nm and 10% at 800 nm. This behavior may be attributed to the relaxation of metastable radiation-induced defects that absorb in the near-infrared region. Notably, this trend is consistent with the behavior observed during the post-irradiation absorbance measurements using spectrophotometry, further confirming the wavelength-specific nature of recovery dynamics. For the Red 4034 dosimeter subjected to a significantly higher dose of 282 kGy, the recovery kinetics appeared fully saturated. At the dosimetry wavelength of 640 nm, only a 1% decrease in RIA was detected after 3 h post-irradiation. The negligible change is likely due to the high dose deposition, which, at constant dose rate, implies a correspondingly longer irradiation time. This extended exposure period allows for significant recombination and migration of radiation-induced defects during irradiation, leading to the in-situ formation of stable color centers and partial annealing of unstable ones. Consequently, the optical signal reaches a near-equilibrium state by the end of the irradiation, resulting in a very limited recovery afterward. In contrast, samples irradiated for shorter durations tend to exhibit higher apparent recovery, as a greater fraction of defect relaxation processes occur post-irradiation rather than during exposure.

Overall, these results suggest a robust temporal stability of dyed-PMMA dosimeters, particularly at their primary dosimetry wavelengths, while slight wavelength-dependent fading can occur in the near-infrared region. Although further study is needed, the low recovery rates seem promising for suitability of these systems for both real-time and post-irradiation dosimetry applications.

### 4.4. Dose estimation

Fig. 11 presents the readout measurements for the three types of dyed PMMA dosimeters (Gammachrome YR+, Amber 3042, and Red 4034) as well as the FD-7 radiophotoluminescent (RPL) dosimeters, plotted against the reference dose to water. Linear regression fits were

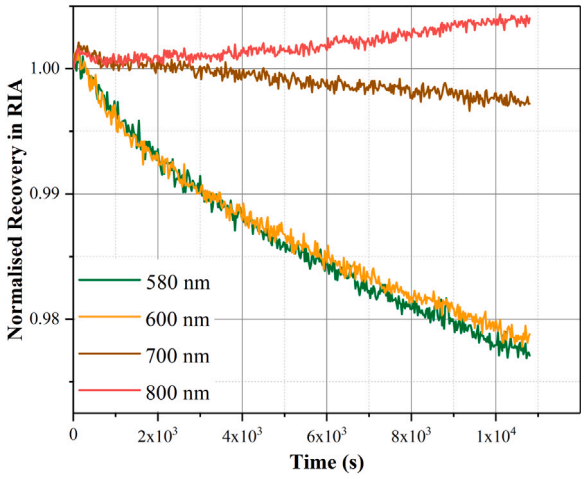


(a) Gammachrome YR+ after 50 kGy

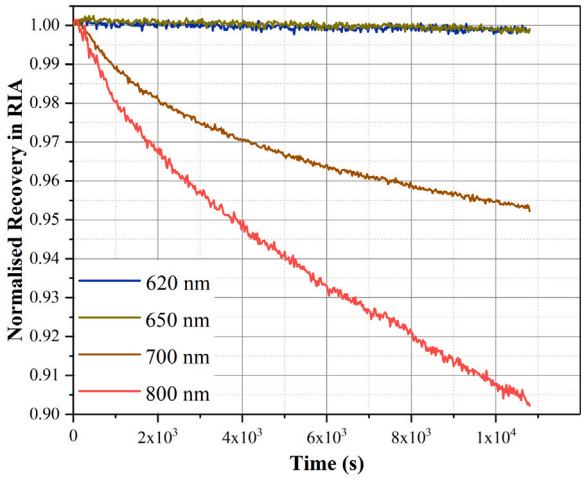


(b) Amber 3042 after 50 kGy

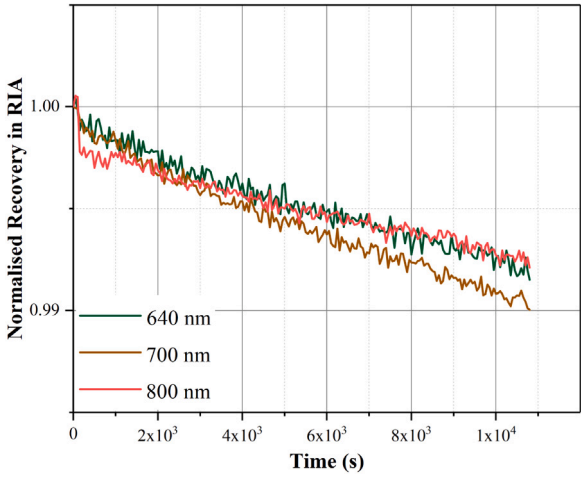


(c) Red 4034 after 282 kGy

**Fig. 10.** Post-irradiation RIA recovery kinetics for (a) Gammachrome YR+, (b) Amber 3042, and (c) Red 4034 PMMA dosimeters over 3 h. Recovery behavior is wavelength-dependent, with high stability observed at primary dosimetry wavelengths.

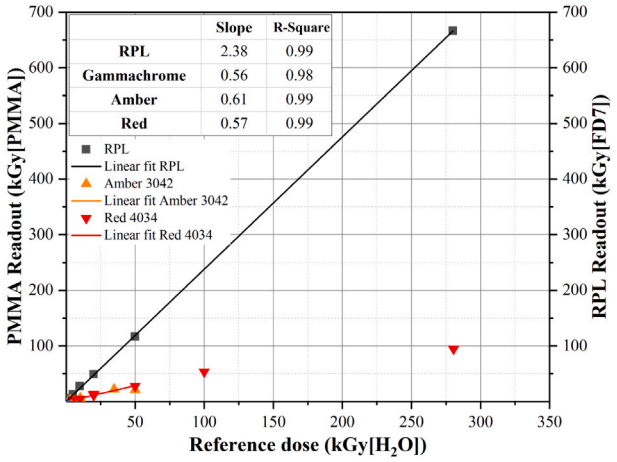


(a) Dose–response curves for Gammachrome YR+, Amber 3042, Red 4034, and FD-7 RPL dosimeters.

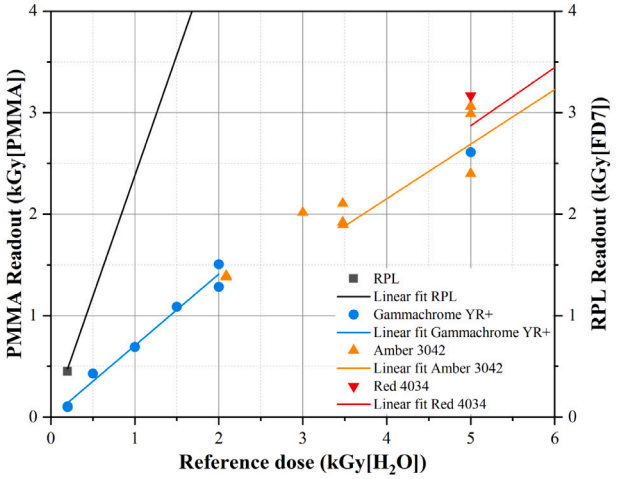


(b) Dose-response curves for the Gammachrome YR+, Amber 3042, Red 4034, and FD-7 RPL dosimeters in the zone of low doses, between 0 Gy and 6 kGy

**Fig. 11.** Dose–response curves: (a) over the entire range of investigated doses, and (b) in the low-dose range for Gammachrome YR+, Amber 3042, Red 4034, and FD-7 RPL dosimeters. Linear fits demonstrate proportionality between dosimeter readout and reference dose across a broad range.

applied to all datasets in range, confirming the proportionality between the measured signal and absorbed dose over their respective sensitivity ranges. The Gammachrome YR+ dosimeter demonstrates accurate dose tracking within its nominal range of 0.1 to 3 kGy, while Amber 3042 and Red 4034 extend the sensitivity range to approximately 30 kGy and 50 kGy, respectively. The RPL dosimeters maintain excellent linearity across the entire dose range and serve as a reliable reference standard for comparison.

The RPL readout and each PMMA dosimeter demonstrated a highly linear response with a coefficient of determination ($R^2$) higher than 0.98. Nonetheless, the response of RPLs and PMMAs with reference dose shows a similar trend.

## 5. Conclusions

This study systematically evaluated the dosimetric performance of dyed-PMMA under high-dose X-ray irradiation. Monte Carlo simulations confirmed that careful management of sample thickness and irradiation geometry ensures sufficiently uniform energy deposition within the PMMA volume, while providing a robust conversion factor to relate dose-to-water to dose-to-PMMA. Post-irradiation absorbance and online radiation-induced attenuation (RIA) measurements revealed a clear dose-dependent optical response, with characteristic wavelength-specific kinetics that reflect the formation and evolution of color centers within the polymer.

Recovery studies showed that the RIA signal remains remarkably stable over several hours, particularly at the nominal wavelengths, with only minor relaxation observed in the near-infrared region. This high temporal stability suggests that dyed-PMMA dosimeters can be suitable for both real-time monitoring and passive dosimetry. A similar trend and perhaps a conversion factor between the dose in RPL and the dose in PMMA can be seen in the responses of RPLs and PMMAs to the reference dose.

## CRediT authorship contribution statement

**Y.Q. Aguiar:** Writing – review & editing, Writing – original draft, Visualization, Validation, Resources, Methodology, Investigation, Formal analysis, Data curation, Conceptualization. **M. Avesani:** Writing – review & editing, Writing – original draft, Visualization, Resources, Methodology, Formal analysis, Data curation. **A. Raj Mandal:** Writing – review & editing, Visualization, Resources, Methodology, Formal analysis, Data curation. **X. Li:** Writing – review & editing, Validation, Resources. **V. Hutanu:** Writing – review & editing, Validation, Resources. **A. Morana:** Validation, Supervision, Methodology. **R. García Alía:** Validation, Supervision, Funding acquisition. **S. Girard:** Writing – review & editing, Validation, Supervision, Funding acquisition. **M. Ferrari:** Writing – review & editing, Validation, Supervision, Resources, Methodology, Investigation, Funding acquisition.

## Declaration of competing interest

The authors declare that they have no known competing financial interests or personal relationships that could have appeared to influence the work reported in this paper.

## Acknowledgments

This work was supported by the French Agence Nationale de la Recherche PROJET N° ANR-22-CPJ2-0117-01.

## Data availability

Data will be made available on request.

## References

Aguiar, Y., et al., 2025. Dose rate effects in Ag-doped metaphosphate glass radiophotoluminescent dosimeters up to MGy range. IEEE Trans. Nucl. Sci. 72 (8), 2570–2577. http://dx.doi.org/10.1109/TNS.2025.3549949.

Attix, F., 1986. Introduction to Radiological Physics and Radiation Dosimetry. Wiley-VCH.

Avesani, M., Ferrari, M., Raj Mandal, A., Aguiar, Y., Garcia Alia, R., Gaillardin, M., Poujols, D., Alessi, A., Cavani, O., Girard, S., 2025. FD-7 dosimeters irradiated in different radiation environments: a comparison between Monte Carlo simulation and experiments. Phys. Status Solidi (A) – Appl. Mater. Sci. (submitted for publication).

Barret, J., 1982. Dosimetry with dyed and undyed acrylic plastic. Int. J. Appl. Radiat. Isot.;(United Kingdom) 33 (11).

Becker, K., 1973. Solid state dosimetry. CRC, Ohio.

Biłko, K., et al., 2023. CERN super proton synchrotron radiation environment and related radiation hardness assurance implications. IEEE Trans. Nucl. Sci. 70 (8), 1606–1615. http://dx.doi.org/10.1109/TNS.2023.3261181.

Boag, J., Dolphin, G., Rotblat, J., 1958. Radiation dosimetry by transparent plastics. Radiat. Res. 9 (6), 589–610.

Camanzi, B., Holmes-Siedle, A., 2008. The race for new radiation monitors. Nat. Mater. 7 (5), 343–345.

Chapiro, A., 1956. Action des rayons gamma sur les polymères à l'état solide-II—Dégradation du polyméthacrylate de méthyle et de l'acétate de cellulose. J. de Chim. Phys. 53, 295–305.

Devic, S., 2011. Radiochromic film dosimetry: past, present, and future. Phys. Medica 27 (3), 122–134. http://dx.doi.org/10.1016/j.ejmp.2010.10.001.

Ferrari, M., Aguiar, Y.Q., Hasan, A., et al., 2024. Characterization of radiophotoluminescence dosimeters under X-Ray irradiation at high doses. IEEE Trans. Nucl. Sci. 71 (8), 1821–1828. http://dx.doi.org/10.1109/TNS.2024.3365272.

Ferrari, M., et al., 2023. "Radiation to materials" at CERN. IEEE Trans. Nucl. Sci. 70 (8), 1580–1586. http://dx.doi.org/10.1109/TNS.2023.3241785.

Fitriana, R., Putri, M., 2020. Study of PMMA dosimeters response against storage temperature and post-irradiation time. In: Journal of Physics: Conference Series, vol. 1436, (1), IOP Publishing, 012053. http://dx.doi.org/10.1088/1742-6596/1436/1/012053.

Girard, S., Kuhnhenn, J., Gusarov, A., Brichard, B., Van Uffelen, M., Ouerdane, Y., Boukenter, A., Marcandella, C., 2013. Radiation effects on silica-based optical fibers: Recent advances and future challenges. IEEE Trans. Nucl. Sci. 60 (3), 2015–2036. http://dx.doi.org/10.1109/TNS.2012.2235464.

Girard, S., Morana, A., Ladaci, A., Robin, T., Mescia, L., Bonnefois, J.-J., Boutillier, M., Mekki, J., Paveau, A., Cadier, B., Marin, E., Ouerdane, Y., Boukenter, A., 2018. Recent advances in radiation-hardened fiber-based technologies for space applications. J. Opt. 20 (9), 093001. http://dx.doi.org/10.1088/2040-8986/aad271.

Girard, S., et al., 2019. Overview of radiation induced point defects in silica-based optical fibers. Rev. Phys. 4, 100032. http://dx.doi.org/10.1016/j.revip.2019.100032.

Girard, S., et al., 2025. PETRA: an experimental platform for X-ray radiation testing of materials and components. In: 15th Symposium SiO2, Advanced Dielectrics and Related Devices. Saint-Étienne, France, URL https://sio2-2025.sciencesconf.org/?lang=en.

Glover, K., Plested, M., Watts, M., Whittaker, B., 1993. A study of some parameters relevant to the response of Harwell PMMA dosimeters to gamma and electron irradiation. Radiat. Phys. Chem. 42 (4), 739–742. http://dx.doi.org/10.1016/0969-806X(93)90363-Y.

Harwell Dosimeters Ltd., 2024. Technical Specification Sheet: Perspex Dosimeters (Harwell). Technical Specification Sheet, Provides technical specifications for Perspex dosimeters and their properties.

Hasan, A., Aguiar, Y., Alía, R.G., Campanella, C., Morana, A., Alem, A., Girard, S., Mandal, A.R., 2024. Online and offline Radiation-Induced Attenuation measurements on FD-7 radiophotoluminescence dosimeters irradiated at high X-ray doses. Radiat. Meas. 177, 107246. http://dx.doi.org/10.1016/j.radmeas.2024.107246.

Huang, D., Hsu, S.-M., 2011. Radio-Photoluminescence Glass Dosimeter (RPLGD). In: Advances in Cancer Therapy. IntechOpen, http://dx.doi.org/10.5772/23710.

Khan, H.M., Ahmad, G., Sattar, A., Durrani, S.K., 1988. Radiation dosimetry using clear PMMA and PVC in the range of 5–45 kGy. J. Radioanal. Nucl. Chem. 125 (1), 1588–2780. http://dx.doi.org/10.1007/BF02041757.

Macha, M., Senajova, D., Giles, T., Calviani, M., Girard, S., Ferrari, M., 2025. Effects of radiation dose on lubricants: A review of experimental studies. ACS Appl. Mater. & Interfaces 17 (10), 14773–14800. http://dx.doi.org/10.1021/acsami.4c21220, PMID: 40013541.

McKeever, S.W., 2022. A course in Luminescence Measurements and Analyses for Radiation Dosimetry. Wiley and Son.

Meyer, A., et al., 2023. Simulation and optimization of optical fiber irradiation with X-rays at different energies. Radiation 3 (1), 58–74. http://dx.doi.org/10.3390/radiation3010006.

Miller, A., Bjergbakke, E., McLaughlin, W.L., 1975. Some limitations in the use of plastic and dyed plastic dosimeters. Int. J. Appl. Radiat. Isot. 26 (10), 611–620. http://dx.doi.org/10.1016/0020-708X(75)90079-4.

Okada, G., et al., 2022. Recent advances in radiophotoluminescence materials for luminescence dosimetry. Jap. J. Appl. Phys. 62 (1), http://dx.doi.org/10.35848/1347-4065/ac9023, Art. no. 010609.

Poludniowski, G., Omar, A., Bujila, R., Andreo, P., 2021a. SpekPy v2. 0—a software toolkit for modeling x-ray tube spectra. Med. Phys. 48 (7), 3630–3637.

Poludniowski, G., et al., 2021b. Technical Note: SpekPy v2.0—a software toolkit for modeling x-ray tube spectra. Med. Phys. 48 (7), 3630–3637. http://dx.doi.org/10.1002/mp.14945.

Pramberger, D., et al., 2022. Characterization of radio-photo-luminescence (RPL) dosimeters as radiation monitors in the CERN accelerator complex. IEEE Trans. Nucl. Sci. 69 (7), 1618–1624. http://dx.doi.org/10.1109/TNS.2022.3174784.

Raj Mandal, A., Ferrari, M., Aguiar, Y.Q., Morana, A., García Alía, R., Hasan, A., Marin, E., Ouerdane, Y., Boukenter, A., Girard, S., 2025. Online X-Ray radiation induced attenuation of RPL dosimeters: Dose rate dependence at high doses. IEEE Trans. Nucl. Sci. 72 (7), 2021–2028. http://dx.doi.org/10.1109/TNS.2025.3546459.

Rieker, V.F., Bateman, J.J., et al., 2025. Radiochromic film dosimetry for VHEE and UHDR: Protocol adaptation and verification at the CLEAR facility. Front. Phys. 13, http://dx.doi.org/10.3389/fphy.2025.1597079.

Sato, T., Iwamoto, Y., Hashimoto, S., Ogawa, T., Furuta, T., Abe, S.-I., Kai, T., Matsuya, Y., Matsuda, N., Hirata, Y., et al., 2024. Recent improvements of the particle and heavy ion transport code system–PHITS version 3.33. J. Nucl. Sci. Technol. 61 (1), 127–135. http://dx.doi.org/10.1080/00223131.2023.2275736.

Yamamoto, T., 2011. RPL dosimetry: principles and applications. In: AIP Conference Proceedings, Vol. 1345, No. 1. Wollongong, Australia, pp. 217–230.